Targeting cellular stress *in vitro* improves osteoblast homeostasis, matrix collagen content and mineralization in two murine models of osteogenesis imperfecta

Nadia Garibaldi [a,b], Barbara M. Contento [a], Gabriele Babini [c], Jacopo Morini [c], Stella Siciliani [d], Marco Biggiogera [d], Mario Raspanti [e], Joan C. Marini [f], Antonio Rossi [a], Antonella Forlino [a,†] and Roberta Besio [a,†]

***a* - Department of Molecular Medicine,** *Biochemistry Unit, University of Pavia, Pavia, Italy*
***b* - Istituto Universitario di Studi Superiori - IUSS,** *Pavia, Italy*
***c* - Department of Physics,** *University of Pavia, Pavia, Italy*
***d* - Department of Biology and Biotechnology,** *University of Pavia, Pavia, Italy*
***e* - Department of Medicine and Surgery,** *University of Insubria, Varese, Italy*
***f* - Bone and Extracellular Matrix Branch,** *NICHD, National Institute of Health, Bethesda, MD 20892, USA*

Corresponding authors. ***aforlino@unipv.it.***
https://*doi.org/10.1016/j.matbio.2021.03.001*

Abstract

Most cases of dominantly inherited osteogenesis imperfecta (OI) are caused by glycine substitutions in the triple helical domain of type I collagen α chains, which delay collagen folding, and cause the synthesis of collagen triple helical molecules with abnormal structure and post-translational modification. A variable extent of mutant collagen ER retention and other secondary mutation effects perturb osteoblast homeostasis and impair bone matrix quality. Amelioration of OI osteoblast homeostasis could be beneficial both to osteoblast anabolic activity and to the content of the extracellular matrix they deposit. Therefore, the effect of the chemical chaperone 4-phenylbutyrate (4-PBA) on cell homeostasis, collagen trafficking, matrix production and mineralization was investigated in primary osteoblasts from two murine models of moderate OI, *Col1a1*$^{+/G349C}$ and *Col1a2*$^{+/G610C}$. At the cellular level, 4-PBA prevented intracellular accumulation of collagen and increased protein secretion, reducing aggregates within the mutant cells and normalizing ER morphology. At the extracellular level, increased collagen incorporation into matrix, associated with more mature collagen fibrils, was observed in osteoblasts from both models. 4-PBA also promoted OI osteoblast mineral deposition by increasing alkaline phosphatase expression and activity. Targeting osteoblast stress with 4-PBA improved both cellular and matrix abnormalities in culture, supporting further *in vivo* studies of its effect on bone tissue composition, strength and mineralization as a potential treatment for classical OI.

Introduction

Bone modelling and remodelling require the anabolic activity of osteoblasts (OBs), which are responsible for the synthesis of the extracellular matrix (ECM) [1]. Bone ECM, mainly consisting of type I collagen with contributions from several non-collagenous molecules, is the scaffold on which mineral deposition and cell interaction occur, thus its integrity is essential to guarantee proper bone structure and biomechanical properties, as well as cell-cell and cell-matrix communication [2–4]. Indeed, many inherited skeletal dysplasias are associated with mutations in bone ECM components and their pathogenic mechanism is generally attributed to impaired ECM assembly and function [5–9]. In the last decade it has been appreciated that bone cellular dysfunction also contributes to pathological mechanisms. Mutated proteins may be retained in the endoplasmic reticulum (ER) causing cellular stress that may affect the clinical outcome [5,7,10–16]. One example of this cellular effect is

the intracellular accumulation of mutant collagen type I in classical osteogenesis imperfecta (OI).

OI is the most common hereditary skeletal dysplasia, characterized by reduced bone mineral density, mild to severe bone deformity and frequent fractures occurring in presence of minor or no trauma [17]. Individuals with OI display a broad phenotypic range, from mild osteoporosis to perinatal lethality sometimes even in the presence of identical mutations, and the molecular basis of this phenotypic variability is still unknown [9,18–20]. Classical OI (types I to IV based on the Sillence classification [21]) is a dominantly inherited disease due to mutations in the *COL1A1* and *COL1A2* genes encoding the α chains of type I collagen. The most common defects are glycine substitutions responsible for the folding delay of the α chains and of their prolonged exposure to the post translational modifying enzymes, thus causing the synthesis of abnormal collagen molecules with increased proline and lysine hydroxylation and hydroxylysine glycosylation [14,22–24]. In cells from many patients and in various OI murine models, the misfolded collagen is partially retained intracellularly, altering cell homeostasis and provoking a cell stress response which could function as a modulator of OI [14,17,25–27]. Indeed, in the OI murine model Brtl, carrying an α1(I)-G349C substitution and having either a moderate or a lethal outcome, the significant difference in expression of ER stress-related proteins indicated involvement of the intracellular machinery in modulating or responding to OI severity, which makes its components potential novel targets for OI therapy [19,28].

Current pharmacological treatments for OI rely almost exclusively on the use of bisphosphonates, a class of antiresorptive drugs inhibiting osteoclast differentiation and/or activity, used in the management of osteoporosis [29]. Despite success in increasing DEXA (dual-energy x-ray absorptiometry) bone density [30–33], the efficacy of these treatments to reduce the fracture risk is controversial and questions about effective dose, cycling intervals and efficacy and safety of long-term use in developing bones of children with OI remain to be answered [34,35]. Thus, the identification of novel targets for new pharmacological approaches is an urgent clinical need for these patients.

4-phenylbutyrate (4-PBA), a chemical chaperone already approved by the FDA as an ammonia scavenger, was used in preclinical and clinical trials to treat diseases caused by intracellular accumulation of misfolded proteins [36–41]. Its chaperone ability was first identified in diseases such as cystic fibrosis [42] and type 2 diabetes associated to obesity [43] where 4-PBA was able to alleviate ER stress and unfolded protein response (UPR) activation, and to restore intracellular trafficking [42,44,45]. We have recently demonstrated that 4-PBA treatment rescues cellular homeostasis through reduction of cell stress in patient fibroblasts carrying mutations in both collagen and non-collagenous genes [26,27] and leads to skeletal improvement in the zebrafish *Chihuahua* model of classical OI [46].

For in depth studies of the effectiveness of innovative therapies, models that recapitulate human anatomy and physiology more faithfully than zebrafish are preferable, and murine models are often the best choice [47,48]. *Col1a1*$^{+/G349C}$ (Brtl) and *Col1a2*+/^{G610C} (Amish) mice are well established models of a classical form of OI, carrying a triple helical glycine substitution in α1(I) and in α2(I) chain, respectively. Brtl and Amish reproduce glycine substitutions previously characterized in OI probands and they model the majority of the patient defects [49–51].

Both mice reproduce the growth deficiency, lower bone mineral density and altered mineral-to-matrix ratio and bone geometry underlying bone deformity and fragility, which are typical of individuals affected by OI [49,52–55]. The imbalance between formation and resorption in bone remodelling, in favour of the latter, is a significant contributor to the bone phenotype in OI. Indeed in the Brtl model, osteoclast number and function are increased, while mineral apposition is decreased during growth, pointing to a decline in osteoblast activity [56]. Brtl mesenchymal stem cells show impaired osteoblastogenesis and a preference towards adipocytic differentiation [28]. Appositional bone growth is also compromised in the Amish model [54], in which osteoblasts are characterized by malfunction, impaired differentiation and lower mineral deposition [14]. Intracellular mutant collagen retention associated with ER cisternae enlargement and altered organization of collagen fibers in the ECM are common features in both models [24,57].

In the present study, primary osteoblasts from Brtl and Amish OI murine models were used to investigate their baseline response to mutant collagen intracellular retention and to evaluate the effect of the chemical chaperone 4-PBA on cellular homeostasis and extracellular matrix deposition.

Results

Osteoblasts homeostasis is altered in OI murine models

In order to investigate the cellular response to the synthesis of mutant collagen in primary OI osteoblasts, we performed qPCR-based transcriptomic analyses evaluating the expression of genes involved in three major stress related pathways: unfolded protein response (UPR), autophagy, and apoptosis. The UPR was strongly activated in both OI murine models, with 77 upregulated genes in Amish mouse and 40 in Brtl (Fig. 1A). The

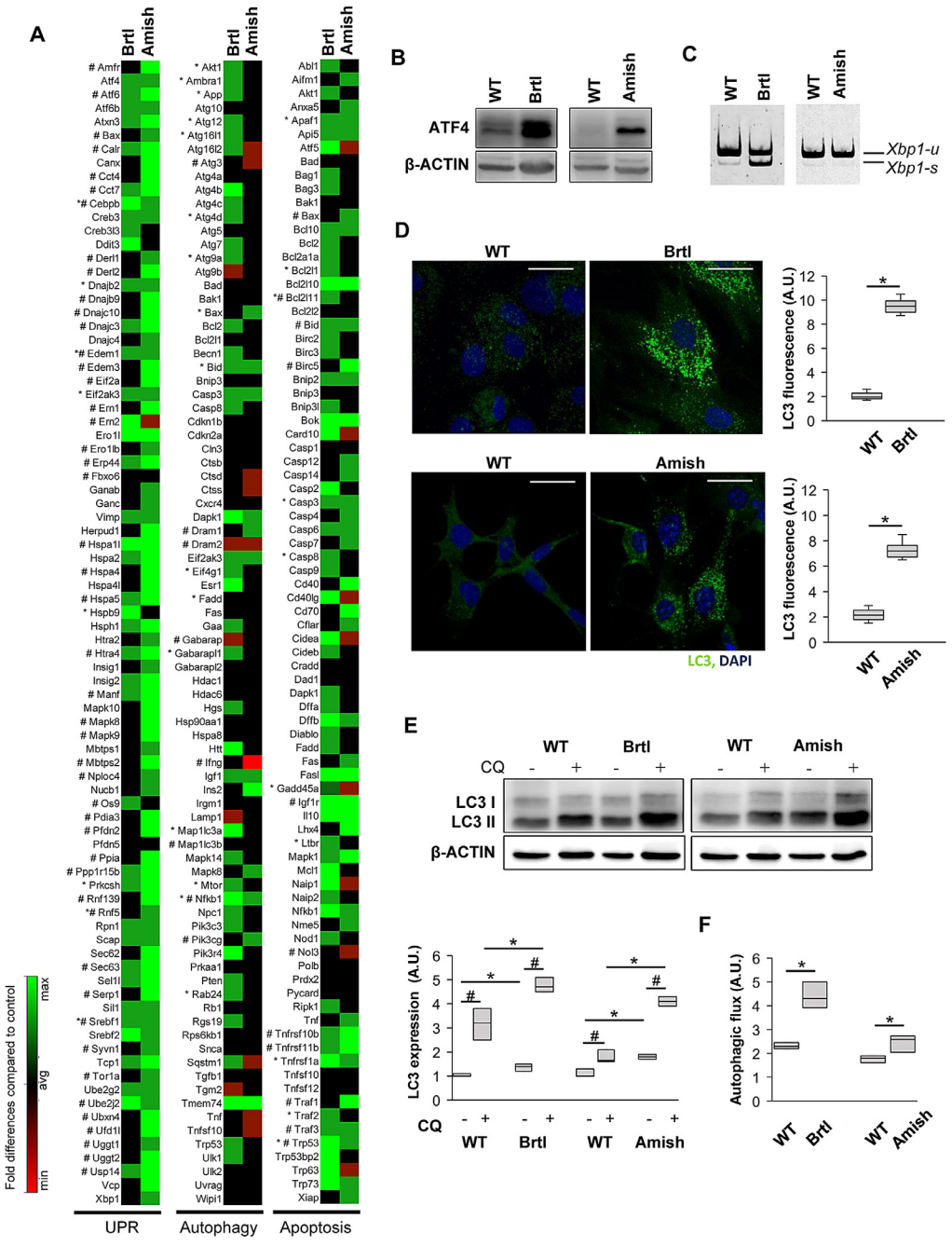

Fig 1. Osteoblasts homeostasis is altered in the Brtl and Amish models. (A) qPCR-based array heat map of relative expression of genes involved in UPR, autophagic and apoptotic pathways in Brtl and Amish OBs. Results are expressed as fold differences compared to control. The upregulation of 40 and 77 genes involved in UPR, 39 and 12 genes involved in autophagy and 54 and 38 genes involved in apoptosis were detected in Brtl and Amish, respectively. *$p<0.05$ WT VS Brtl; # $p<0.05$ WT VS Amish. (B) Representative ATF4 western blot image. The protein was upregulated in both OI models. (C) RT-PCR amplification of *Xpb1* mRNA from control (WT) and mutant OBs. The spliced *Xbp1* form (*Xbp1-s*) of *Xbp1* transcript (*Xbp1-u*) was detected in Brtl. (D) Representative immunofluorescence images and quantification of LC3 in WT and mutant OBs. Quantitation of the total area of punctate signal per cell indicated the activation of autophagy. Nuclei were stained with DAPI. Scale bar: 20 μm. *$p<0.05$ WT VS mutant. (E) Representative LC3 western blot performed on WT and mutant cell lysates obtained following chloroquine (CQ) incubation. β-actin was used for normalization. Bands quantitative analysis revealed LC3-II upregulation in chloroquine treated Brtl and Amish OBs compared to their controls. *$p<0.05$ WT VS mutant; # $p<0.05$ untreated VS chloroquine treated. (F) Autophagic flux, evaluated as the ratio between LC3II level in chloroquine treated samples and the untreated ones, was increased in both models. *$p<0.05$ WT VS mutant.

expression of several chaperones was enhanced in both models. *Cct7*, encoding a chaperone involved in folding newly translated polypeptides, and *Calr,* encoding the ER luminal protein calreticulin that binds misfolded proteins and prevents their progression through the secretory pathway, displayed increased expression compared to controls. Also upregulated were genes encoding for proteins involved in protein disulphide isomerization (*Erp44*) and ER quality control of polypeptide folding (*Edem1, Prkcsh, Rpn1*). In addition, numerous members of the heat shock protein family were upregulated, specifically *Dnajb2, Dnajc3, Hspa1l, Hspa2, Hsph1* and, importantly, *Hspa5*, encoding for the ER chaperone and UPR initiator BIP (Fig 1A). Interestingly, the upregulated genes included UPR players *Atf6* (ATF6 branch) and *Eif2ak3* (PERK branch), with its effector *Atf4.* ATF4 protein was also increased in both models, confirming PERK branch activation (Fig. 1B), while IRE1α-mediated splicing of *Xbp1* was detectable only in Brtl OBs (Fig. 1C), indicating that in this model cell stress triggers a more general response involving multiple UPR branches. The expression of numerous genes involved in ubiquitination processes and in misfolded proteins degradation (*Amfr, Herpud1, Ubxn4, Uggt1, Uggt2, Usp14, Vimp, Vcp*) was increased in Amish cells (Fig. 1A).

Autophagy was activated in both models, although only Brtl mice displayed a substantial upregulation of autophagic genes (Fig. 1A). Among the 39 upregulated genes in Brtl OBs, many were involved in autophagosome formation and growth. In particular, we observed enhanced expression of several family members of autophagy related genes (ATG), including the key autophagic factors *Atg12, Atg16l1 and Atg16l2*, involved in autophagic vesicles formation. Furthermore, we observed augmented level of *Map1lc3a*, encoding for the terminal autophagic marker LC3 that participates to autophagosome membrane expansion. Immunofluorescence analyses revealed an increased level of LC3 (Fig. 1D) and western blot performed on cell lysates following chloroquine treatment showed significantly increased LC3II expression in both models (Fig. 1E). Importantly, the autophagic flux, calculated as the ratio between LC3II level in chloroquine treated and untreated samples [58,59], was increased in both models (Fig. 1F).

Finally, apoptosis activation was evaluated, revealing both in Brtl and Amish a considerable number of upregulated genes (Fig. 1A). Several death domain receptor genes, encoding initiator proteins that trigger the apoptotic cascade, in particular several members of Tumor Necrosis Factor (TNF) receptor superfamily *Tnfrsf10b, 11b* and *1a*, were increased in both models. Brtl cells also displayed activation of the two death domain receptors *Fadd*, recruited by TNF proteins and activators of initiator caspases, and *Dapk1*, involved in autophagy-dependent apoptosis regulation.

Interestingly, anti-apoptotic factors were also upregulated, predominantly in Brtl cells, such as genes of the Bcl-2 family (*Bcl10, Bcl2, Bcl2a1a, Bcl2l1, Bcl2l11*) together with their enhancers *Bag1, Bag3* and *Bnip2* genes encoding the BCL-2 interacting proteins. Different members of the caspase family, responsible for the apoptotic cascade, were increased in both Brtl and Amish. Apoptosis initiators such as *Casp2, Casp8* and *Casp9* were activated preferentially in Brtl, while the effector caspases *Casp4*, Casp7, *Casp12* and *Casp14* were activated in Amish OBs. Importantly, *Casp6*, one of the main effector caspases, and *Casp3*, the caspase in charge of apoptosis execution, were upregulated in both models (Fig. 1A). Although the pathway was triggered in both models, Brtl cells had increased expression of a larger number of genes (Brtl $n = 54$; Amish $n = 38$). Immunofluorescence of cleaved caspase 3 (Fig. 2E) and FACS quantification of apoptotic cells with annexin V and propidium iodide confirmed the activation of apoptosis in both models (Brtl 1.94 ± 0.43 fold differences respect to WT, $p < 0.05$; Amish 1.55 ± 0.48 fold differences respect to WT, $p < 0.05$, **Supplementary fig. 1**).

4-PBA improves osteoblasts homeostasis by alleviating cellular stress

To investigate whether modulation of cell stress would rescue cellular homeostasis, OBs were treated with the chemical chaperone 4-PBA. Following drug administration, consistent changes in the gene expression pattern of both models was observed (Fig. 2A). In particular, BIP-encoding gene *Hspa5* and its nucleotide exchange factor *Sil1*, together with the effectors of the PERK UPR branch (*Eif2ak3, Atf4*), were downregulated, revealing a beneficial effect of 4-PBA in reducing ER stress response. OBs from the two models displayed a normalization or a decrease in the level of expression of chaperones such as *Calr*, calreticulin, and *Tcp1*, a member of the chaperonin-containing TCP1 complex (CCT) that assists protein folding. In Brtl cells in particular, the normalization of protein disulphide isomerase *Erp44* and, interestingly, the upregulation of quality control protein-coding genes such as *Uggt1* and *Uggt2,* was observed (Fig. 2A). In Amish OBs, 4-PBA led to a more pronounced general reduction of UPR genes expression, decreasing chaperones (*Calr, Canx, Cct4, Cct7*), proteins involved in folding and quality control (*Dnajb2, Dnajb10, Dnajc3, Dnajc4),* and the majority of heat shock proteins (*Hspa1l, Hspa4, Hspa5, Hsph1*). Of note, the expression of *Serpinh1*, encoding for the collagen-specific molecular chaperone heat shock protein 47 [60], was also reduced by the treatment (Fig. 2B).

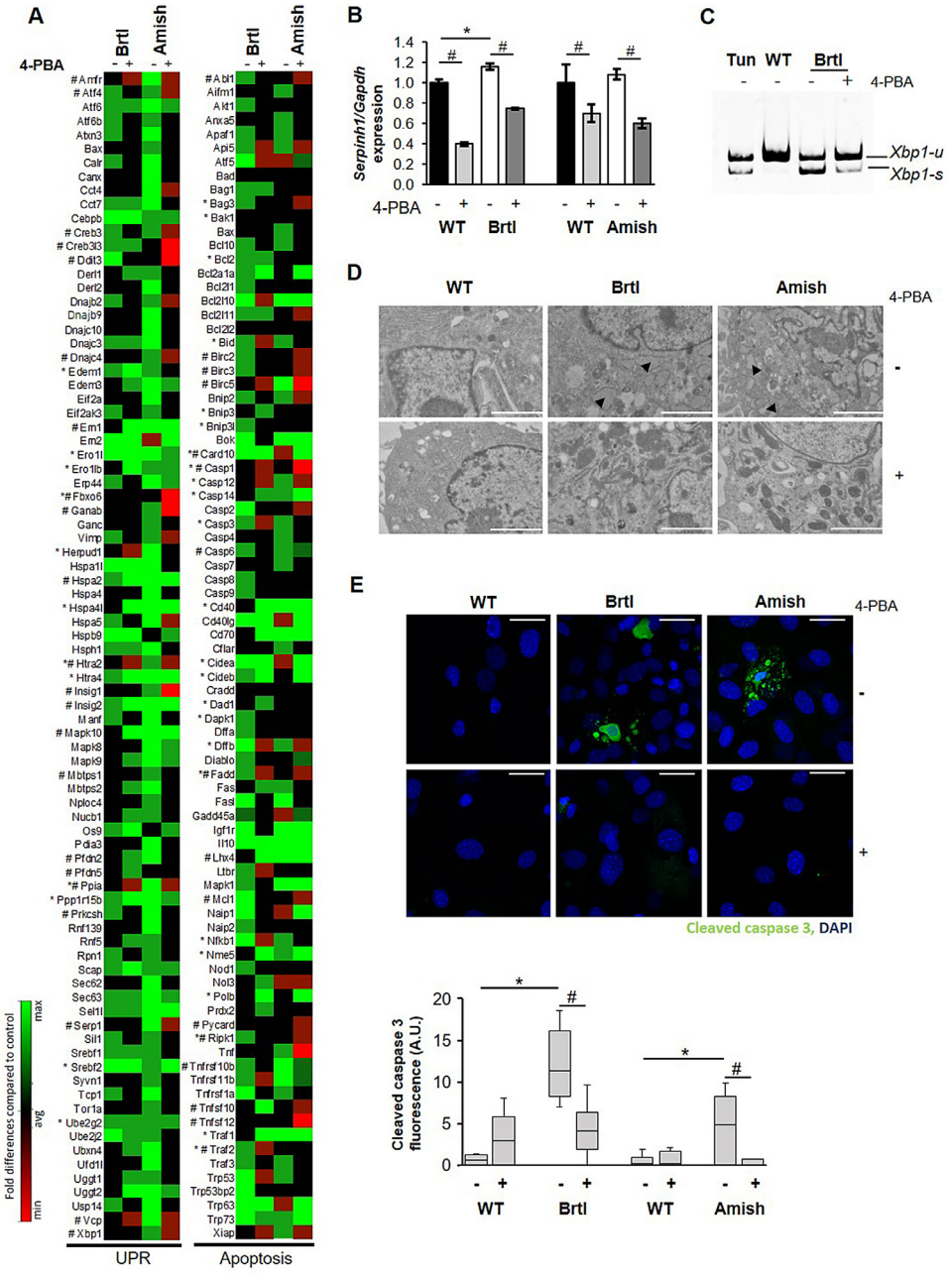

Fig 2. 4-PBA ameliorates Brtl and Amish osteoblasts homeostasis. (A) qPCR-based array heat map of relative expression of genes involved in UPR, autophagic and apoptotic pathways in Brtl and Amish OBs in the absence (-) or presence (+) of 4-PBA. Results are expressed as fold differences compared to control. 4-PBA mainly reduced or normalized the upregulated genes. *$p<0.05$ 4-PBA treated Brtl VS control; #$p<0.05$ 4-PBA treated Amish VS control. (B) qPCR analysis of *Serpinh1* expression in mutated and control OBs cultured in the absence (−) or presence (+) of 4-PBA. The drug reduced *Serpinh1* expression in all samples. *$p<0.05$ WT VS mutant, #$p<0.05$ 4-PBA treated VS untreated. (C) RT-PCR amplification of *Xbp1* mRNA from control and Brtl untreated (-) and 4-PBA (+) treated OBs. *Xbp1-s* is reduced by 4-PBA. cDNA from OBs treated with the stress inducing compound tunicamycin were used as positive control for ER stress. (D) Transmission electron microscopy representative images of OI OBs in absence (-) or presence (+) of 4-PBA. The analyses revealed ER enlargement (arrowhead) in mutant cells that was rescued by 4-PBA treatment. Scale bar: 2 μm. (E) Representative immunofluorescence images and quantification of cleaved caspase 3 in WT and mutant OBs in absence (-) or presence (+) of 4-PBA. Quantitation of the total area of punctate signal indicated increased cleaved caspase 3 level in mutant OBs, pointing to the activation of apoptosis. 4-PBA treatment reduced the apoptotic marker signal in mutated cells. Nuclei were stained with DAPI. Scale bar: 2 μm. *$p<0.05$ WT VS mutant, #$p<0.05$ 4-PBA treated VS untreated.

In addition, the expression of all the previously overexpressed genes promoting ubiquitination and proteasomal degradation (*Amfr, Derl1* and *2, Edem1, Herpud1, Nploc4, Nucb1, Rnf139, Rnf5, Sec62, Syvn1, Ube2j2, Ubxn4, Ufd1l, Usp14, Vcp Vimp*) was lowered or restored to control level, suggesting that the need of a degradation pathway for unfolded proteins was diminished (Fig. 2A). Validation of array results pointed out that *Xbpl* splicing, increased in untreated Brtl OBs, was significantly reduced upon 4-PBA administration, further indicating the efficacy of the compound in alleviating cell stress (Fig. 2C). The impact of 4-PBA on expression of stress genes was also mirrored by substantial improvement in cellular morphology. The ER cisternae, enlarged in mutant cells from both models, appeared normalized after treatment, as revealed by transmission electron microscopy imaging (TEM) (Fig. 2D).

Along with UPR genes, we demonstrated the beneficial effect of 4-PBA on apoptotic gene expression. We observed a substantial decrease in the number of relevant upregulated genes in both models following 4-PBA administration (Fig. 2A). Expression of TNF family genes (*Tnfrsf10b, Tnfrsf11b, Tnfrsf1a* in Brtl; *Tnf, Tnfrsf1a* in Amish) was lowered by 4-PBA, together with genes that mediate the apoptotic cascade, in particular caspases (*Casp2, 3, 6, 8* and *9* in Brtl; *Casp1, 2, 3, 4, 7* in Amish). Furthermore, Brtl cells displayed reduced expression levels of death domain receptors such as *Dapk1* and *Fadd* (Fig. 2A). Expression of apoptosis regulation factors was also reduced in both models upon treatment, in particular decreased expression of *Bcl* genes and their regulators suggests a general mitigation of the pathway activation. Reduction of cleaved caspase 3 expression by immunofluorescence analysis (Fig. 2E) further supported the findings at the transcript level that 4-PBA administration attenuates the apoptotic cascade in OI OBs from both murine models.

4-PBA reduces intracellular protein aggregation and stimulates secretion

Since TEM imaging highlighted a considerable ER enlargement in OI samples (Fig. 2D), we investigated the effect of 4-PBA on ER proteostasis by treating cells with the protein aggregate-binding fluorescent molecule Thioflavin T (ThT) [61]. Enhanced ThT fluorescence was found in Brtl and Amish OBs compared to controls, demonstrating the intracellular accumulation of misfolded material (Fig. 3A). Following 4-PBA treatment, mutated cells exhibited reduced ThT fluorescence. The reduction of ER protein accumulation (Fig. 3A) was further supported by increased general protein secretion (Fig. 3B), also detectable in WT cells.

Scanning electron microscopy (SEM) analysis was performed to visualize the 4-PBA effect on cellular morphology. While control OBs appeared as a flat layer, Brtl and Amish untreated cells had an enlarged and rugged globular shape that was normalized following 4-PBA administration (Fig. 3C). The rounded Amish cells were characterized by an abnormal accumulation of calcium, colocalizing with phosphorus and oxygen, as revealed by energy-dispersive X-ray spectroscopy (Fig. 3D).

Procollagen accumulation in ER is diminished upon 4-PBA administration

4-PBA stimulation of protein secretion leaves open the question about its specific effect on collagen molecules. A strong ER procollagen accumulation was observed in Brtl and Amish cells compared to controls by its colocalization with the PDI marker and not with the Golgi marker GM130 (Fig. 4, **Supplementary fig. 2**). The increased LAMP1 signal and COLI-LAMP1 colocalization in Brtl and Amish cells are also indicative of the cellular attempt to cope with procollagen accumulation by enhancing the degradative pathway (Fig. 4**, Supplementary fig. 3**). Importantly, incubation with 4-PBA substantially prevented intracellular procollagen accumulation, as demonstrated by normalized intracellular procollagen signal in the two models and substantially reduced COLI-PDI and COLI-LAMP1 colocalization (Fig. 4). No difference in collagen overmodifications was detectable upon treatment based on collagen electrophoretic analysis (**Supplementary fig. 4**).

Collagen matrix incorporation and maturation are improved by 4-PBA treatment

Since 4-PBA led to a substantial reduction of intracellular procollagen content in mutated cells, we examined *Col1a1* expression by qPCR at different time points during mineralization and collagen protein synthesis by ^{3}H proline incorporation. 4-PBA reduced collagen expression in Brtl, Amish and control OBs, both at the transcript and protein level (Fig. 5A, B). Nevertheless, the gene expression of collagen type V and of the small-leucine rich proteoglycan biglycan, which regulate collagen fibrillogenesis, was not negatively affected by the treatment (**Fig. 5C and Supplementary Fig. 5**). Importantly, the treatment with 4-PBA specifically increased collagen secretion in mutated cells (Fig. 5D). Matrix analyses revealed that the incorporation of collagen into mutant decellularized matrix increased after treatment in comparison to treated controls (Fig. 5E). In untreated samples SEM imaging showed that control cells were surrounded by an abundant matrix of uniform collagen fibers, on which small proteoglycans were deposited in an organized fashion (**Supplementary Fig. 6**), while the matrix deposited by mutated cells appeared less

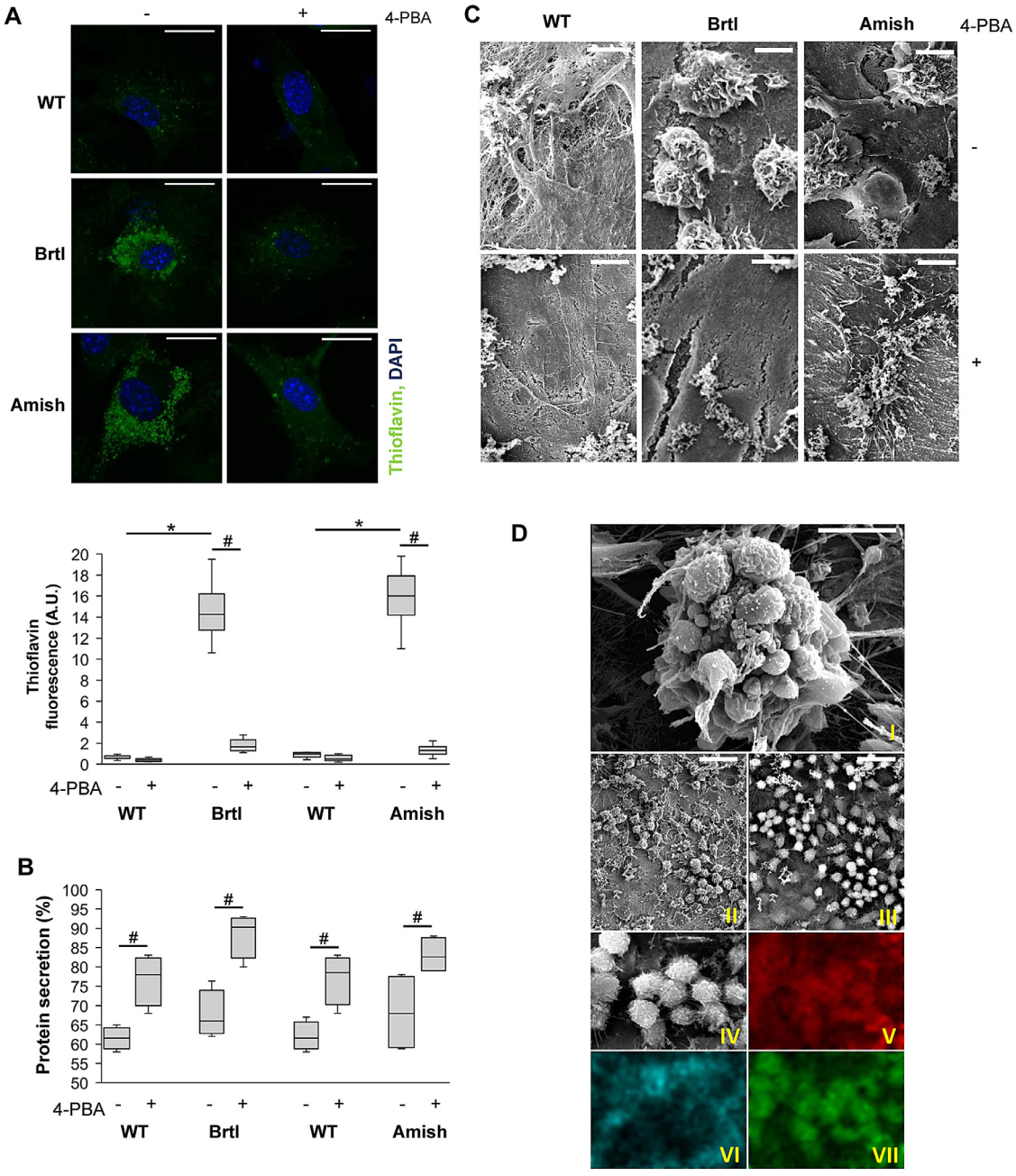

Fig 3. 4-PBA reduces intracellular protein aggregation and stimulates secretion. (A) ER proteostasis was evaluated by Thioflavin T (ThT) immunofluorescence. Representative images and ThT quantification are shown. ThT fluorescence was increased in mutant cells compared to control, highlighting the intracellular accumulation of misfolded proteins. 4-PBA treatment significantly reduced ThT fluorescence, proving its ability in stimulating proteostasis. Scale bar: 20 μm. (B) Protein secretion was evaluated in absence (-) or presence (+) of 4-PBA. The drug stimulated protein secretion in WT, Brtl and Amish cells. (C) Scanning electron microscopy representative images of Brtl, Amish and control OBs in the absence (−) or presence (+) of 4-PBA. Morphology analyses showed the presence of rounded cells in mutant samples respect to the dark flat layer of control cells. 4-PBA improved mutant cells morphology. Scale bar: 10 μm. (D) Amish OBs morphology was evaluated by SEM. **I.** The analyses revealed the presence of rounded cells with a rough surface. Scale bar: 5 μm. **II.** Rounded cells. Scale bar: 25 μm. **III.** Ca^{2+} accumulation in Amish OBs is highlighted by a higher signal in back-scattered electron imaging. Scale bar: 25 μm. **IV.** A cluster of Amish OBs in conventional secondary electrons is shown. Magnification 1200X. **V-VI-VII.** Energy-dispersive X-ray spectroscopy showed in false colour the corresponding mapping of calcium (red), sodium (light blue) and phosphorus (green). Note the perfect colocalization of calcium and phosphorus, compared with the unrelated distribution of sodium. *$p<0.05$ WT VS mutant, # $p<0.05$ 4-PBA treated VS untreated.

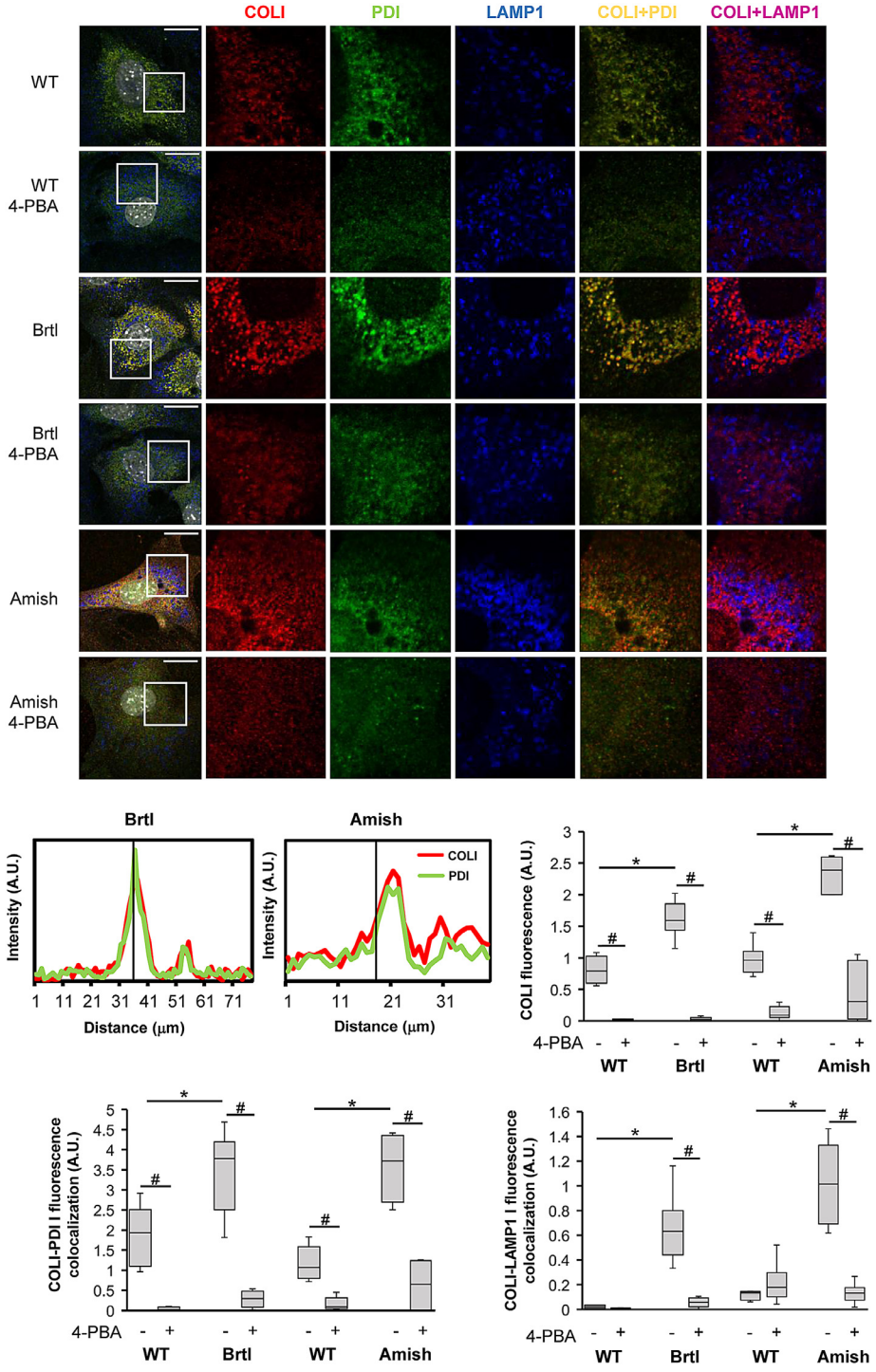

Fig 4. Collagen accumulation in the ER in OI OBs is relieved upon 4-PBA administration. (A) Representative images and quantification of multiple immunofluorescences of collagen (COLI), the ER marker PDI and the lysosomal marker LAMP1 on mutant and control OBs in the absence (−) or presence (+) of 4-PBA. Collagen accumulation was evident in mutant cells and reduced by 4-PBA treatment. Collagen molecules colocalized with PDI indicating their retention in the ER that was reduced by the treatment. LAMP1 expression was increased in mutant samples and reduced by the treatment. Importantly, collagen colocalization with LAMP1 in mutant OBs was rescued by 4-PBA treatment. Nuclei were stained with DAPI. Scale bar: 15 μm. Colocalization graphs of COLI-PDI signal in Brtl and Amish OBs is shown below the images indicating two overlapping peaks. *$p<0.05$ WT VS mutant, # $p<0.05$ 4-PBA treated VS untreated.

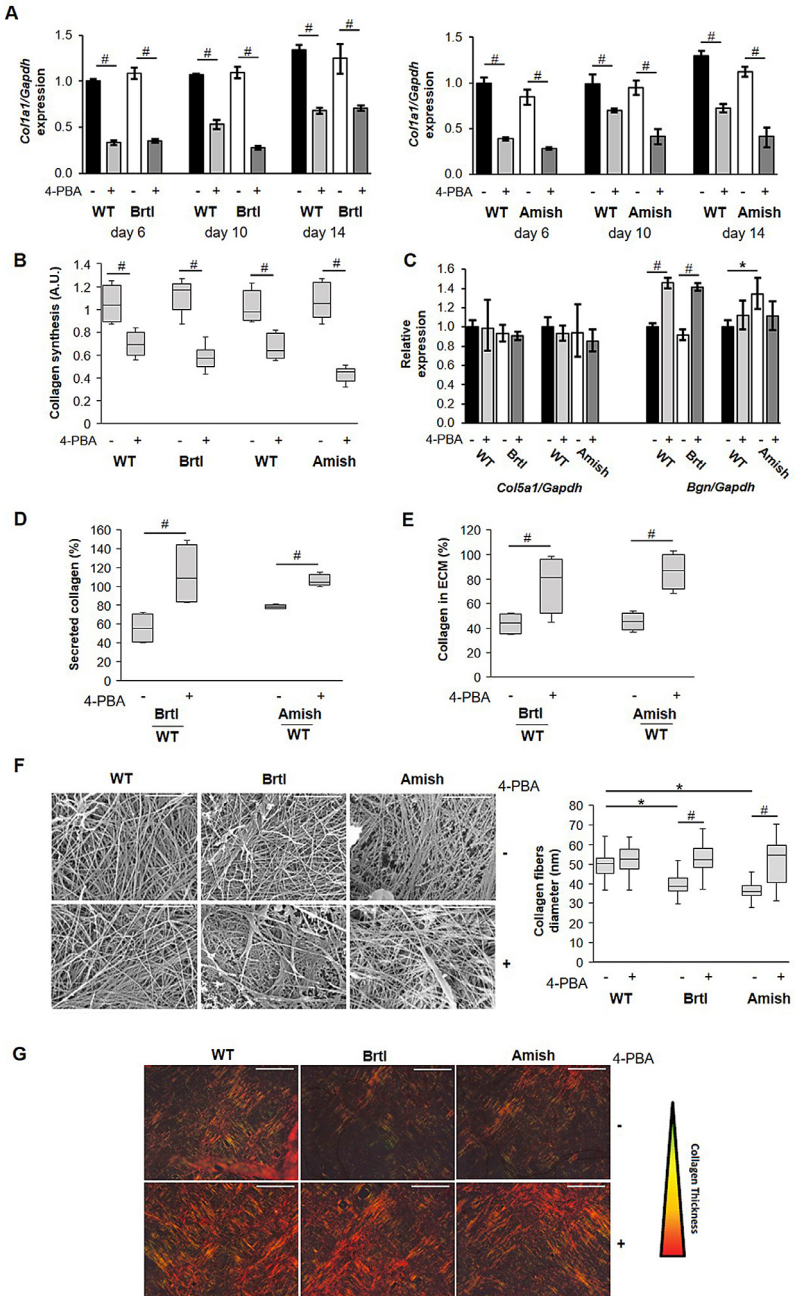

Fig 5. Collagen maturation and incorporation into the matrix are improved by 4-PBA treatment. (A) qPCR analysis of *Col1a1* expression in mutated and control OBs at 6, 10 and 14 days of culture in osteogenic media in the absence (−) or presence (+) of 4-PBA. The drug reduced collagen expression in all samples at each time point. (B) Collagen synthesis in mutated and control OBs in standard culture conditions was evaluated by ^{3}H proline incorporation assay in the absence (−) or presence (+) of 4-PBA. The drug administration diminished collagen content in all samples, but more consistently in control. (C) qPCR analysis of *Col5a1* and *Bgn* expression in mutated and control OBs at 14 days of culture in osteogenic media in the absence (−) or presence (+) of 4-PBA. *Col5a1* expression was unchanged by the treatment while the drug increased *Bgn* expression in Brtl cells. (D) Collagen secretion was also evaluated. At basal level, mutated cells presented impaired secretion compared to WT, while treatment with 4-PBA specifically increased collagen secretion in both Brtl and Amish OBs. (E) The amount of collagen incorporated into the ECM was evaluated in mutated and control OBs grown in osteogenic media for 21 days in absence (-) or presence (+) of 4-PBA. Collagen content was reduced in both Brtl and Amish samples but that upon treatment the incorporation of collagen in mutant decellularized matrix increased with respect treated control. (F) SEM images of mutant and control collagen fibrils produced by OBs. Mutated fibrils appeared thinner and their size was increased when treated with 4-PBA. Scale bar: 2 μm. (G) Sirius red staining highlighting collagen fibers in OBs matrix. Immature fibers are green, mature fibers are red. While mutated untreated cells present more immature fibers than control, 4-PBA treatment improves collagen fibrils maturation. Scale bar: 200 μm. *$p<0.05$ WT VS mutant, # $p<0.05$ 4-PBA treated VS untreated.

organized, and thinner immature fibrils were present (Fig. 5F). 4-PBA administration in mutant cells resulted in a more mature matrix (Fig. 5G) characterized by the presence of thicker collagen fibrils (Fig. 5F).

4-PBA promotes mineralization in Brtl and Amish OBs

The effect of 4-PBA on matrix mineralization was also investigated. Mineral staining by alizarin red highlighted an impaired mineral deposition in mutated cells, as well as a boost in mineral deposition after 4-PBA administration in both models (Fig. 6A). Accordingly, the activity of the alkaline phosphatase (ALP) enzyme was increased upon treatment (Fig. 6B). Enhanced expression of the early osteoblast differentiation markers zinc-finger transcription factor (*Osx*) and alkaline phosphatase (*Alp*) was also stimulated by 4-PBA during mineralization (Fig. 6C, D). Indeed, an increased level of acetylation of histone H3 was found in Brtl and Amish OBs upon treatment (**Supplementary Fig. 7**), supporting the drug effect on *Osx* and *Alp* at the transcriptional level.

Discussion

In the present work, we have addressed the consequences of the presence of mutant collagen in OI osteoblasts and its role as a target for chaperone-based therapy to ameliorate cell homeostasis and matrix quality (Fig. 7). Indeed, collagen type I misfolding and intracellular accumulation is known to happen in cells of some OI patients and in OI animal models [13,14,26,28,50,62-66]. The consequent activation of unfolded protein response and apoptosis was demonstrated in patients' fibroblasts [26,27,62,63], highlighting a malfunction associated to intracellular mutant collagen with a potential role in OI clinical pathology. Here we investigated the stress response to intracellular procollagen retention in primary osteoblasts from two dominant OI murine models, Brtl and Amish, carrying glycine substitutions in α1 or α2 type I collagen chains, respectively. Osteoblasts represent indeed the cells of election to study OI pathogenesis since, besides secreting collagen, they are in charge of matrix mineralization [67,68]. Furthermore, although the primary sequence of type I collagen in skin and bone is identical, bone collagen has a unique pattern of post-translational modifications, resulting in a tissue-specific chemical profile of pyridinoline and pyrrole crosslinking and in a more delayed electrophoretic migration, suggesting a possible cell-specific metabolism associated to mutant collagen [65,67−71].

UPR, autophagy and apoptosis are activated in Brtl and Amish osteoblasts as consequence of mutant collagen retention

OI bone cells from both models activated UPR, autophagy, and finally apoptosis in response to mutant collagen intracellular accumulation, reproducing findings from patients' fibroblasts [26]. A common altered expression pattern of molecular chaperones and heat shock proteins is shared by both models, as well as the UPR activation through the PERK branch. The IRE1α branch is enhanced in Brtl OBs, but unchanged in Amish, although we cannot exclude IRE1α cascade activation in this model, given the upregulation of several *Xbp1-s* target genes, including *Dnajc3, Dnajb9, Edem1* and *Serp1* [72]. Interestingly, in OI fibroblasts carrying α1 glycine substitutions, the IRE1α upregulation was detected only in 2 out of the 5 analysed cases carrying mutation in the C-terminal half of the collagen molecules, whereas all patients' fibroblasts with glycine substitution in α2 chain showed IRE1α upregulation with the exception of the cells with G640C substitution, for which no UPR activation was detected [26]. Taken these data together, it seems that while PERK is confirmed as the main UPR branch activated by mutant collagen retention, the activation of IRE1α may be mutation or cell type dependent. A higher number of autophagic and apoptotic genes were deregulated in Brtl, in which higher level of the terminal apoptotic marker was also present, compared to Amish, whereas the expression of UPR genes was mostly affected in Amish. The differential intracellular response may be due to the stoichiometry of collagen, indeed 75% of mutant collagen is synthetized in cells carrying α1 (I) mutations and 50% in presence of α2(I) defects.

The response to ER stress is an important modifier of disease severity in many human pathologies [73], including skeletal diseases such as those with mutations in the ECM components matrilin 3, COMP and collagen X [5−8,11,74,75]. For instance, the onset of a metaphyseal chondrodysplasia phenotype in mice, in which ER stress was artificially triggered in hypertrophic chondrocytes, demonstrated the potential for a direct pathological role of ER stress in the etiology of the disease [76]. Studies in mouse models indicate that the effect of ER stress signaling (ERSS) and the nature of the cellular strategies induced to ameliorate pathological ER stress are crucial factors in determining cell fate and clinical disease features [10]. Importantly, ERSS can affect cellular proliferation and differentiation, and cell-

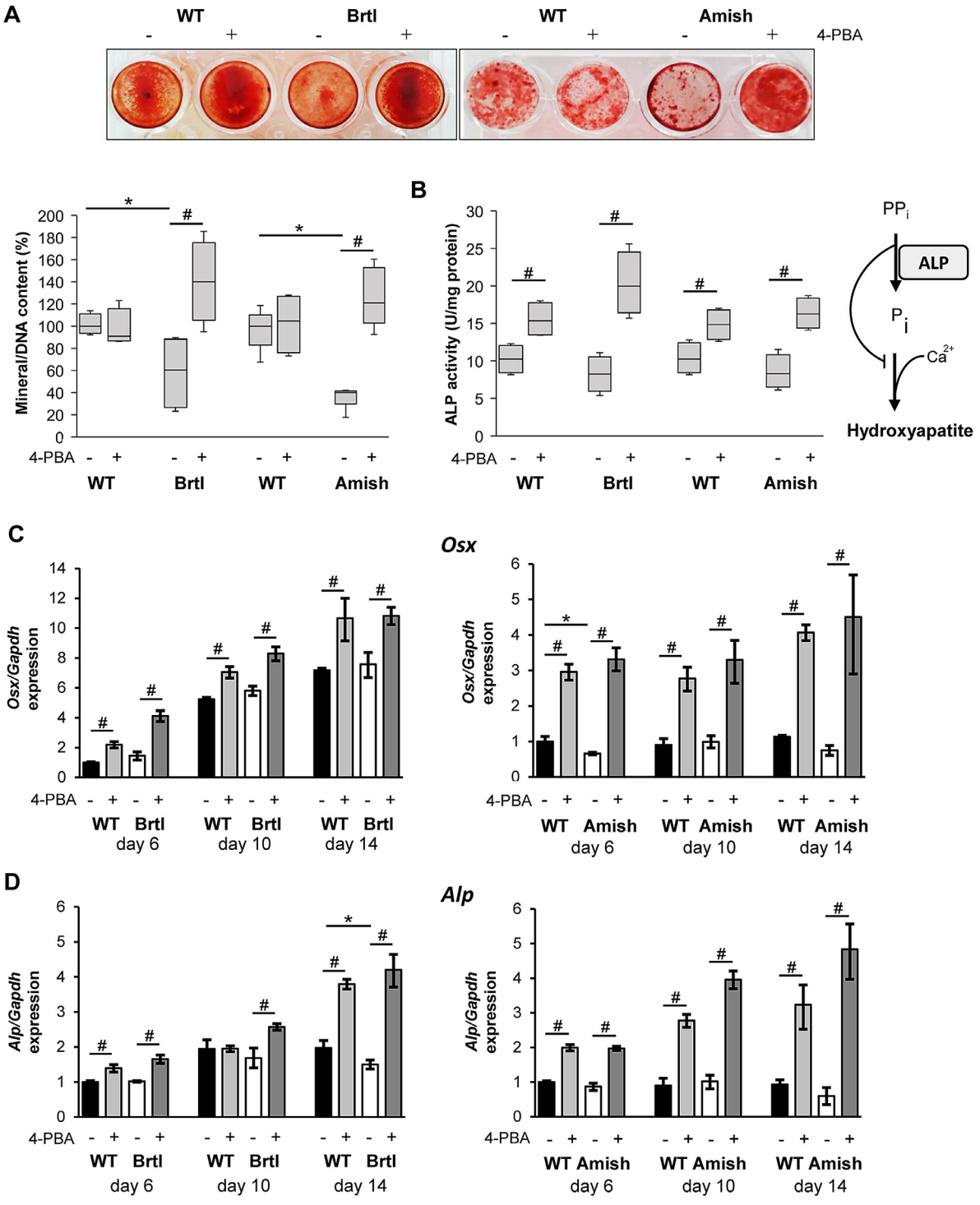

Fig 6. 4-PBA promotes mineralization in Brtl and Amish OBs. (A) Alizarin red staining of primary OBs cultured in osteogenic medium in absence (−) or presence (+) of 4-PBA. OBs mineral content was quantified. A decreased mineral staining in Brtl and Amish cells was evident. Upon 4-PBA treatment, an increased mineral content was found, demonstrating the positive action of the drug in stimulating OBs mineralization. (B) ALP activity in osteogenic medium in absence (−) or presence (+) of 4-PBA was evaluated by enzymatic assay. A significant enhancement of ALP activity was detected in mutant and control cells following 4-PBA administration. (C-D) Real time PCR analyses of *Alp* and *Osx* expression in Brtl and Amish OBs at day 6, 10 and 14 of culture in osteogenic medium in absence (−) or presence (+) of 4-PBA. 4-PBA promoted genes expression in mutant and WT cells at all time points analyzed. *$p<0.05$ WT VS mutant, # $p<0.05$ 4-PBA treated VS untreated.

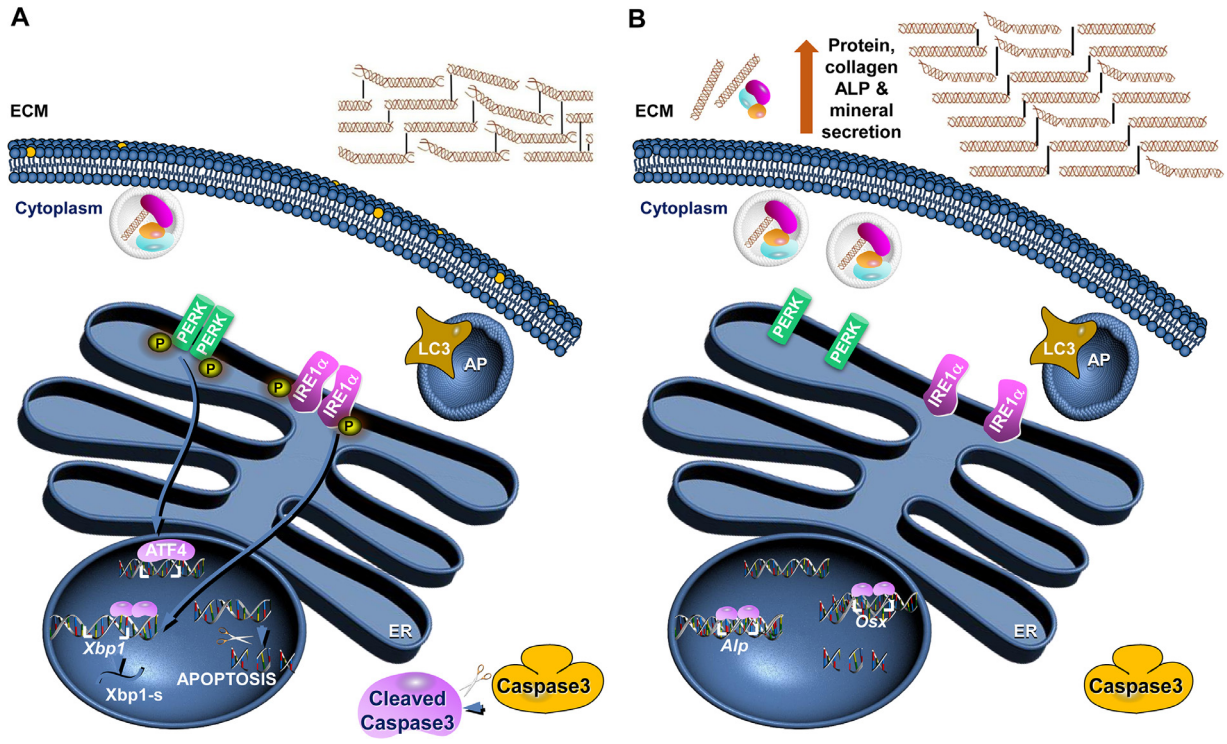

Fig 7. Schematic view of the mechanisms activated by OI OBs to face intracellular collagen retention and highlighting the molecular mechanisms of action of 4-PBA. (A) Mutated collagen I is partly secreted in the ECM, where it impairs its structure and functions, and partly retained in the ER, causing ER stress and the consequent activation of UPR through protein kinase R (PKR)-like endoplasmic reticulum kinase (PERK) and inositol-requiring enzyme 1 α (IRE1α) branches. Phosphorylated PERK activates its effector ATF4, that translocates to the nucleus where it regulates gene expression. IRE1α activation leads to the alternative splicing of its effector X-box binding protein 1 (*Xbp1*), that works as a transcriptional activator in its spliced form. Intracellular protein accumulation also stimulates the degradative pathway autophagy, as revealed by the increased expression of its terminal marker LC3, present on autophagosome (AP) membrane. Prolonged activation of UPR induces apoptosis, in particular through the cleavage of the main apoptotic executor Caspase 3. A hallmark of apoptosis activation is the flipping of the phospholipid phosphatidylserine (indicated by yellow dots in the cell membrane) from the inner leaflet of the plasma membrane to the outer one. (B) 4-PBA reduces the activation of UPR and apoptosis markers and stimulates general protein secretion, clearing the ER from accumulated material. The drug exerts its effect on collagen, specifically, by promoting its secretion and incorporation into the ECM. Increased *Osx* and *Alp* expression following treatment, as well as increased ALP activity, denote 4-PBA stimulatory effect on OBs differentiation and mineralization activity.

autonomous adaptation strategies can generate a spectrum of cellular consequences, ranging from recovery to death. ERSS alters both the transcriptome and proteome of a cell, affecting its metabolic status and, likely, impairing its secretory abilities with a secondary extracellular effect that may contribute to the phenotypic variety of the disease. Indeed, in the Brtl mouse, differential expression of chaperones, proteasomal subunits, metabolic enzymes, and proteins related to cellular fate revealed a superior ability to adapt to cellular stress in surviving Brtl mutant mice compared to lethal mice with the same molecular defect, and indicated the potential relevance of the cell response to the stress as an OI phenotype modulator [19,77]. Based on these observations, targeting ER stress holds intriguing potential as a strategy to mitigate the phenotype in bone diseases caused by mutations in ECM components.

4-PBA relieves OI osteoblasts stress improving cell homeostasis

4-PBA has recently gained increasing attention for its chaperone-like activity [78] and its efficacy in lowering ER stress markers and apoptosis in several non-skeletal [36–40,45] and skeletal diseases, including OI [12,26,27,79]. We recently demonstrated that 4-PBA treatment alleviates cell stress in dominant and recessive OI fibroblasts by restoring ER cisternae size, switching off activation of the PERK UPR branch and normalizing the expression of the apoptotic marker cleaved caspase 3 [26,27]. Here we proved for the first time the beneficial

effects of 4-PBA in OBs, providing evidences for its relevant direct effect on collagen. Of note, we showed that 4-PBA treatment reduced the procollagen accumulation in the ER, thanks both to its ability to down regulate collagen synthesis and to increase collagen secretion. No difference in collagen overmodification after treatment was evident by electrophoretic analysis, suggesting there was likely no or limited effect on the delay in folding caused by the collagen substitution and, thus, level of post translational modification. A consistent effect on collagen secretion upon 4-PBA administration was previously shown only in fibroblasts from a patient with a very C-terminal α1-G859S substitution, while a milder effect was reported in cells carrying other mutations spread along the N-terminal and mid-helical portion of the triple helical domain [26]. Interestingly, Brtl and Amish mutations fall at different helical positions, α1-G349 and α2-G610 respectively, nevertheless 4-PBA significantly stimulate collagen secretion in both. It is, therefore, tempting to speculate a stronger effect of the drug on cells, such as OBs, characterized by higher collagen production. It is important that 4-PBA action extends also to general protein secretion, reducing protein aggregates in osteoblasts in both models, as was reported in fibroblasts from both dominant and recessive patients [26,27]. An intriguing mechanism has recently been proposed to explain the action of 4-PBA in regulating protein secretion. The COPII coat protein SEC24, a component of the secretory path necessary for the translocation of proteins from the ER to the Golgi, was recently identified as a 4-PBA target. The authors showed that 4-PBA action on SEC24 promotes COPII packaging of ER proteins, stimulating sorting and reducing trafficking stringency [80]. It will be interesting to evaluate this mechanism in OI cells as well.

4-PBA improves OI extracellular matrix quality

ECM amelioration upon ER stress targeting has been already attempted in skeletal disease and, for instance, in a mouse model of short-limbed dwarfism by treatment with carbamazepine, a compound stimulating autophagy and proteasomal degradation and, consequently, lowering misfolded proteins accumulation in the ER and UPR activation [81]. In this model the treatment was able to ameliorate the skeletal phenotype supporting the validity of the target. Whether and how 4-PBA administration affects ECM was still a puzzling question. The use of this drug in mice in presence of type IV collagen mutation was beneficial in lowering ER stress markers and increasing collagen IV secretion and incorporation into kidney basement membrane but without improving its ultrastructure [82]. In a very recent work, 4-PBA has been shown to reduce the amount of misfolded type I collagen in ECM laid down by OI fibroblasts and to either augment iPSCs differentiation ability toward OBs or favour mineral deposition in fibroblast-derived iPSCs differentiated to OBs [83].

Importantly, here we demonstrated for the first time a positive effect of 4-PBA on ameliorating the quality of ECM laid down by primary osteoblasts. Our data demonstrated that, upon 4-PBA incubation, collagen fibers deposited by mutant OBs appear more mature. This may positively affect collagen-non-collagenic proteins interaction, and further investigation will be necessary to shed light on overall ECM organization. Indeed, even if the mutations in the two models are not located in any of the three collagen major ligand binding regions (MLBRs), they fall in regions involved in the interaction with small proteoglycans [84,85]. In particular, the α1-G349 falls into the binding site region for decorin and for keratan sulfate PGs and α2-G610 into the binding site for COMP and for dermatan/chondroitin sulfate PGs.

Even though 4-PBA reduced collagen expression, a selective effect on mutated cells was evident. Together with collagen deposition, mineralization is another fundamental process of bone formation that was impaired in Brtl and Amish OBs *in vitro*. 4-PBA administration promoted ALP enzyme activity, stimulated mineral deposition and increased calcium deposits in both models' OBs, providing the molecular bases for the increased bone mineralization in the treated OI zebrafish model Chihuahua [46]. Of relevance, 4-PBA was reported to act as a histone deacetylase inhibitor, allowing the transcription of osteogenetic genes, promoting cell proliferation/maturation in OBs cultures [86–89]. An increased level of acetylation of histone H3 was found in Brtl and Amish OBs upon treatment, supporting a transcriptional effect of the drug on *Osx* and *Alp* expression.

In conclusion, our findings demonstrated the efficacy of 4-PBA both in restoring OI osteoblasts homeostasis, and in improving extracellular matrix collagen organization and mineralization. This *in vitro* investigation paves the way for further *in vivo* studies in animal models to prove the promising roles of chemical chaperons in the treatment of OI and to determine their effects on bone tissue strength, cellularity, mineralization and growth.

Materials and methods

Mouse strain and genotyping

CD1/129Sv/B6 *Col1a1*$^{+/G349C}$ (Brtl) [49] and CD1/CH3/B6 *Col1a2*$^{+/G610C}$ (Amish) [50] mice, carrying a heterozygous G349C substitution in the collagen I α1 chain and a G610C substitution in the collagen I α2 chain, respectively, were used for this study. The

Amish mice were kindly provided by Prof Charlotte Phillips, University of Missouri-Colombia, USA. Mutant mice and WT littermates were maintained under standard experimental animal care protocol following Italian Laws in the centralized animal facility of the University of Pavia, Italy. All the experiments were approved by the OPBA (Office for the Animals Welfare) of the University of Pavia and by the Italian Ministry of Health (protocol n. 243/2018-PR, 27/03/18), complied with the ARRIVE guidelines and were carried out in accordance with the EU Directive 2010/63/EU for animal experiments. Genomic DNA was extracted from tail clip and genotyping was performed by PCR as previously reported [49,50].

Calvarial osteoblasts culture

Murine osteoblasts were isolated from 2-4 days old WT and mutant pups [90]. Cells from at least three animals with the same genotype were pooled together to obtain a sufficient number for experiments. After sacrifice, calvariae were removed, cleaned from fibrous tissues and sutures, washed twice with Phosphate Buffer Saline (PBS) at 37 °C for 10 min in a shaker water bath and sequentially digested with 200 U/mL collagenase type II (GIBCO) at 37 °C for 15 min. Cells obtained from the first two digestions were discharged, whereas cells from digestions 3, 4 and 5 were passed through a 70 μm polypropylene mesh filter and cultured in α-Modified Eagle's Medium (α-MEM, Lonza) supplemented with 10% fetal bovine serum (FBS, Euroclone), 50 μg/ml sodium ascorbate (Fluka) 4 mM glutamine (Euroclone), 100 μg/ml penicillin and streptomycin (Euroclone) at 37 °C in humidified atmosphere containing 5% CO_2. Cells were used at passage 1.

For each experiment, except when differently stated, $1.5 \times 10^4/cm^2$ were plated, cultured with no media change with the addition every other day of 50 μg/ml ascorbic acid and harvested after 5 days. For drug treatment, cells were incubated for 15 h with 5 mM 4-phenylbutyrate (4-PBA, Sigma-Aldrich) before harvesting. To inhibit lysosome-autophagosome fusion, cells were incubated with 10 μM chloroquine (Sigma-Aldrich) for 6 h. To induce ER stress, osteoblasts were treated with 2 μg/mL tunicamycin for 16 h before harvesting. For mineralization studies, cells were cultured in α-MEM with 20% FBS, antibiotics, 100 μg/ml L-ascorbic acid (Sigma-Aldrich), and 10 mM β-glycerophosphate (Sigma-Aldrich) (osteogenic medium). The medium was changed three times a week. Harvest was performed at different time points, as detailed below.

Transcriptomic analyses

Total RNA was extracted from OBs from 3 independent cells preparations per genotype in absence or presence of 4-PBA with QIAzol Lysis Reagent (Qiagen) and purified by miRNeasy Mini Kit (Qiagen) according to the manufacturer's protocol. RNA concentration was determined by nanodrop and its integrity was verified on agarose gel. cDNA synthesis was performed using RT^2 First Strand kit (Qiagen) according to the manufacturer's protocol. The expression of key genes involved in UPR, autophagy and apoptosis was evaluated by Unfolded Protein Response RT^2 Profiler PCR Array, Autophagy RT^2 Profiler PCR Array and Apoptosis RT^2 Profiler PCR Array (Qiagen) using RT^2 SYBR Green Mastermix, according to the manufacturer's instructions. Arrays were performed on the QuantStudio3 thermocycler (Thermo Fisher). Data were analyzed using GeneGlobe Data Analysis Center software (Qiagen), five housekeeping genes (*Actb, b2m, Gapdh, Gusb, Hsp90ab1*) were used for normalization.

Xbp1 splicing analyses

cDNA from control and mutant cells, cultured in absence or presence of 4-PBA or in presence of the stress inducer tunicamycin, was used for PCR amplification across the region of the *Xbp1* cDNA (NM_013842.3) containing the intronic target of IRE1α ribonuclease using 0.4 μM sense (nt 720-740; 5'-GAACCAGGAGTTAAGAACACG-3') and antisense (nt 924-905; 3'-AGGCAACAGTGT CAGAGTCC-5') primers. Reactions were cycled as follows: 3 min at 95 °C, followed by 35 cycles of 95 °C for 40 s, 60 °C for 45 s and 72 °C for 40 s, lastly a 10 min extension at 72 °C was applied. The *Xbp1* unspliced form (205 bp) and the *Xbp1* spliced form (179 bp) were visualized on 8% TBE acrylamide gel. Biological triplicates were performed.

Protein lysates

Cultured osteoblasts were collected in PBS upon scraping, centrifuged at 1000 × g for 4 min, lysed and sonicated in RIPA buffer (150 mM NaCl, 1% IGEPAL® CA-630, 0.5% sodium deoxycholate, 0.1% SDS, and 50 mM Tris, pH 8) supplemented with protease inhibitors (5 μl/ml phenylmethanesulfonylfluoride and 2 mM Na_3VO_4, pH 10). Proteins were quantified by QuantumProtein Bicinchoninic Protein Assay Kit (Euroclone). Bovine serum albumine (BSA) (Sigma-Aldrich) was used as standard.

Western blot

Proteins from osteoblasts lysates (10 μg) were run on SDS-PAGE in 10% and 15% acrylamide gels for ATF4 and LC3, respectively. The proteins were electrotransferred to a PVDF membrane (GE Healthcare) at 100 V for 2 h on ice in 19 mM Tris-HCl, 192 mM glycine and 20% (v/v) methanol. The

membranes were then blocked with 5% (w/v) BSA in 20 mM Tris-HCl, 500 mM NaCl, pH 7.5 (TBS), 0.05% (v/v) Tween-20 (Sigma-Aldrich) (TBS-T) at RT for 1 h. The membranes were incubated with 1:1000 primary antibody against the specific proteins LC3A/B (Cell Signaling), ATF4 (Novus Biological) in 5% BSA in TBS-T o/n at 4 °C. The secondary antibody (Cell Signaling) was added at dilution of 1:2000 in 5% BSA in TBS-T for 1 h at RT. The signal was detected by ECL western blotting detection reagents (GE Healthcare) and images were acquired with ImageQuant LAS 4000 (GE Healthcare), using the ImageQuant LAS 4000 1.2 software. Band intensities were evaluated by densitometry, using ImageQuant TL analysis software. Biological triplicates were performed. For each gel, the intensity of the control band was set equal to one and the expression of the mutant samples was expressed as fold difference. Actin was used for protein loading normalization.

Fluorescence activated cell sorting (FACS)

Apoptosis was evaluated by Fluorescence Activated Cell Sorting (FACS) using Annexin V/Dead Cell Apoptosis Kit (Invitrogen), following manufacturer's instruction in four independent OBs preparations. Cells incubated with 20 μM thapsigargin (Sigma-Aldrich) for 24 h in serum-free α-MEM were used as positive control for the activation of apoptosis. Samples were analyzed by Attune NxT Acoustic Flow Cytometer (Thermo Fisher), 1×10^4 events for each sample were considered measuring the fluorescence emission at 515−545 nm (FITC) and 675−715 nm (PI), to avoid fluorescence spillover.

Transmission electron microscopy analysis

For transmission electron microscopy analysis, following trypsinization osteoblasts were centrifuged at 1000 $\times$ g for 3 min. Incubation with 1% glutaraldehyde in culture medium for 2 h at room temperature (RT) was used to fix the cell pellet, which was then rinsed in PBS and in H_2O. Finally, OBs were fixed in 2% (w/v) OsO_4 in H_2O for 2 h at RT, rinsed in distilled water and embedded in 2% agarose. The specimens were dehydrated in acetone and infiltrated with Epoxy resin overnight (o/n) and polymerized in gelatin capsules at 60 °C for 48 h. Thin sections (60−70 nm thick) were cut on a Reichert OM-U3 ultramicrotome with a diamond knife and collected on 300-mesh nickel grids. Saturated aqueous uranyl acetate by lead citrate was used to stain the grids. A Zeiss EM900 electron microscope, operated at 80 kV with objective aperture of 30 μm was used for the analysis.

Thioflavin T labelling

OBs from three independent preparations were plated on sterile glass coverslips (Marienfeld) in 24 well plate and cultured for 4 days before incubation with 5 μM Thioflavin (ThT, Sigma-Aldrich) for 15 h in presence or absence of 4-PBA. Cells were then fixed with 4% paraformaldehyde (PFA) in PBS for 20 min at RT. 4',6-diamidino-2-phenylindole (DAPI, Sigma-Aldrich) was used for staining nuclei. Images were acquired by SP8- Leica confocal microscope (Leica). The total area of punctate signal per cell was measured using the Leica software LAS4.5.

Protein secretion

OBs from three independent preparations were plated in 24 well plate and labelled with 5 μCi/ml [^{35}S] EXPRESS35S Protein Labeling Mix (PerkinElmer) in α-MEM without L-methionine, L-cystine, and L-glutamine for 1 h at 37 °C. The precipitation of the medium and cell layer total proteins was carried out with 10% trichloroacetic acid. Following acetone washing the pellet was resuspended in 60 mM Tris-HCl, pH 6.8, 10% sodium dodecyl sulphate. The radioactivity (counts for minute, CPM) of the samples was quantified using a liquid scintillation analyzer (TRI-CARB 2300 TR). The percentage of protein secretion was calculated based on the ratio between the CPM in the media and the CPM in medium and cell layer.

Immunofluorescence

2×10^4 OBs were plated on sterile glass coverslips (Marienfeld) in 24 well plate. After 4 days cells were treated for 15 h with 5 mM 4-PBA.

LC3 and cleaved caspase 3

For LC3 immunofluorescence, after 5 days cells were treated for 6 h with 10 μM chloroquine. On day 5, the medium was removed and cells were fixed with 10% neutral buffered formalin for 30 min at RT, washed 3 times with PBS and blocked 1 h in 1% BSA in PBS containing 0.3% TritonX100. LC3 primary antibody (Cell Signaling) and cleaved caspase 3 primary antibody (Cell Signaling) were used at 1:500 dilution in 1% BSA, 0.3% TritonX100 in PBS and the incubation was carried out o/n at 4 °C. Following PBS washing, cells were incubated with secondary antibody (AlexaFluor 488 conjugated F(ab') fragment anti-rabbit IgG, Immunological Sciences) diluted 1:2000 for LC3 and 1:400 for cleaved caspase 3, respectively, in 1% BSA, 0.3% TritonX100 in PBS for 2 h at RT.

Collagen intracellular co-localization

For collagen localization studies, the medium was removed and cells were fixed for 45 min in 10% neutral buffered formalin and blocked with 0.5% BSA, 0.05% saponin, 50 mM NaCl and 15 mM glycine pH 7.4. For collagen colocalization with the ER marker PDI and with the Golgi marker GM130, cells were sequentially incubated o/n with COLI (1:100, *COL1A1 Antibody (SP1.D8) - DSHB (Developmental Studies Hybridoma Bank* directed against the N-terminal propeptide of the α1 chain of collagen I), PDI (1:200, Cell Signaling) and AlexaFluor 647 conjugated anti-GM130 antibody (1:100, BD Pharmingen) antibodies. The secondary antibodies AlexaFluor 546 goat anti- mouse IgG (Invotrogen) and AlexaFluor 488 conjugated F(ab') fragment anti- rabbit IgG (Immunological Sciences) were used at 1:400 dilution. For collagen colocalization with the ER marker PDI and with the lysosome marker LAMP1, cells were sequentially incubated o/n with COLI (1:100, SP1D8 hybridoma bank in mouse), LAMP1 (1:200, Abcam) PDI AlexaFluor 647 conjugate (1:100, Invitrogen) antibodies. The secondary antibodies AlexaFluor 546 anti-mouse IgG (Immunological Sciences), and AlexaFluor 488 conjugated F(ab') fragment were used at 1:400 dilution. All the antibodies were diluted in the previously described blocking buffer.

For both experiments, nuclei were stained with DAPI and images were acquired by confocal microscope TCS SP8 (Leica). The total area of punctate signal per cell and signals colocalization were measured by the Leica software LAS 4.5.

Scanning electron microscopy analysis

OBs were plated on sterile glass coverslips and cultured for 14 days with and without 2.5 mM 4-PBA. Cells were fixed for 1 h in Karnovsky fixative (8% paraformaldehyde, 0.4 M cacodylate buffer, 25% glutaraldehyde, 5% calcium chloride) and dehydrated in ethanol and hexamethyldisilazane. The specimens were mounted on appropriate stubs with a colloidal silver glue, gold coated with an Emitech K550 sputter-coater and observed with a Philips XL-30 FEG scanning electron microscope (Philips XL30FEG) fitted with secondary electron (SE) and backscattered electron (BSE) probes, and with an EDAX Sirion 200/400 dispersive X-ray spectroscopy apparatus. Elemental maps were obtained on selected specimens by X-ray dispersive spectroscopy and filtered using Adobe Photoshop.

Collagen analysis

To analyze the effect of 4-PBA on collagen synthesis, cells were labelled for 15 h in absence or presence of 5 mM 4-PBA using 28.57 μCi of ^{3}H-Pro/ml. Collagen extraction from the media and cell layer was performed as previously reported [91]. Collagen was resuspended in Laemmli buffer (62 mM Tris-HCl, pH 6.8, 10% glycerol, 2% sodium dodecyl sulphate, 0.02% bromophenol blue) and the radioactivity (counts for minute, CPM) was measured using a liquid scintillation analyzer (PerkinElmer TRI-CARB 2300 TR). For collagen steady state method see Supplementary materials.

Mineralized matrix decellularization and collagen quantification

Matrix decellularization was performed in four independent OBs preparations for each genotype as described in [92]. Briefly, cells were cultured for 21 days in osteogenic medium to allow matrix deposition. Following PBS washing, the matrix was decellularized by incubation for 1 h in 50 mM tris-HCl buffer pH 8.0 containing 2 M KCl and 0.2% TritonX-100. The decellularized matrix was extensively washed with 10 mM Tris-buffer pH 8.0 and DNA extraction was performed to confirm decellularization. Collagen extraction and quantification from medium and decellularized matrix was performed using Sircol^{TM} Soluble Collagen Assay (Biocolor), according to the manufacturer's protocol.

Mineralization assays and alkaline phosphatase activity

On day 21 of culture in osteogenic medium, cells were fixed in 10% formalin solution neutral buffered (Sigma-Aldrich) for 1 h and alizarin red staining was performed. Cells were incubated with 58 mM Alizarin Red S pH 4.1-4.3 (Merck) for 45 min. Mineral extraction was carried out by 10% acetic acid extraction and absorbance was measured at 405 nm [93]. Alizarin Red standards (30 μM to 4 mM) were used for calibration curve. DNA was used for normalization.

For the measurement of ALP activity, cells were maintained in osteogenic medium for 21 days in osteogenic media. ALP activity was measured in OBs' media using an alkaline phosphatase detection kit (Abnova) following manufacturer's instruction and normalized to total protein content.

Gene expression analysis by real time PCR

On day 6, 10 and 14 of culture in osteogenic medium, total RNA was extracted from three independent OBs preparations for each strain using QIAzol® Lysis Reagent (Qiagen) according to the manufacturer's protocol. RNA concentration was determined by Nanodrop. DNase digestion was performed using DNA-Free Kit DNase Treatment & Removal (Invitrogen). cDNA was synthetized using High Capacity cDNA Reverse Transctiption kit (Applied Biosystems). qPCR was performed on the QuantStudio3 thermocycler (Thermo Fisher) using

PowerUp Syber Green Master Mix (Applied Biosystems) with custom primers for *mSerpinh1, mCol5a1, mCol5a2, mBgn*, m*Alp* and m*Osx* with m*Gapdh* as normalizer (primers sequences available upon request), and using Taqman Universal PCR Master Mix No Amp Erase UNG to analyze m*Col1a1* expression (Mm00801666_g1) with m*Gapdh* (Mm99999915_g1) as normalizer. All reactions were performed in triplicate. Relative expression levels were calculated using the ΔΔCt method.

Sirius red staining

Sirius red staining was performed to evaluate the organization of the collagen fibers [94,95]. OBs were plated on sterile glass coverslips (Marienfeld) and after 4 days cells were treated for 15 h with 5 mM 4-PBA. On day 5, the medium was removed and cells were fixed with 10% neutral buffered formalin for 30 min at RT, rinsed in PBS and H_2O and then stained for 1 h with 0.1% sirius red (Direct Red-80, Sigma-Aldrich) in saturated aqueous solution of picric acid. The specimens were then washed once in H_2O for 5 min and twice in acidified water for 20 s, they were dehydrated in ethanol, washed twice in xylene for 1 min and mounted on Superfrost® Plus slides (VWR) with DPX Mountant for histology (Sigma-Aldrich). To evaluate Sirius red birefringence, stained cells were analyzed under polarized light by LeicaDM2500 equipped with L ICT/P polarizer and a digital color camera LEICA DFC295 (Leica).

Statistical analysis

Biological triplicates for each genotype and treatment were performed. Quantitative variables were expressed as mean ± standard deviation (SD). One-way repeated measures ANOVA was applied to evaluate genotype and treatment effect followed by post-hoc tests with the Bonferroni's correction. All data passed tests for normality and equal variance. A p value < 0.05 was considered significant.

Declaration of Competing Interest

None

Acknowledgments

We thank Dr. Patrizia Vaghi and Dr. Amanda Oldani, Centro Grandi Strumenti, University of Pavia, Italy, for the confocal analysis support; the animal facility "Centro di servizio per la gestione unificata delle attività di stabulazione e di radiobiologia" of the University of Pavia, Pavia, Italy to host the animals; the OPBA of the University of Pavia for supporting in animal protocol drawing up.

Author's contributions

Conceptualization: A.F., R.B.; Methodology: N.G., B.C., G.B., J.M., S.S., M.B., M.R., J.M., A.R., A.F., R.B.; Formal analysis: N.G., M.R., M.B., A.F., R.B.; Resources: A.R., M.R., M.B., A.F., R.B.; Data curation: N.G., A.F., R.B.; Writing original draft: N.G., A. F., R.B.; Writing - review & editing: all the coauthors; Supervision: A.F., R.B.; Project administration: A.F., R.B.; Funding acquisition: A.F., R.B.

Our colleague G.B. sadly passed away before manuscript submission.

Funding

This work was supported by Italian Ministry of Education, University and Research (MIUR) [Dipartimenti di Eccellenza (2018-2022)] to A.F. and by Fondazione Cariplo (2016-0417) to R.B.

Supplementary materials

Supplementary material associated with this article can be found, in the online version, at doi:10.1016/j.matbio.2021.03.001.

Received 7 January 2021;
Received in revised form 26 March 2021;
Accepted 26 March 2021

Keywords:
Collagen;
Osteogenesis imperfecta;
Endoplasmic reticulum stress;
Chemical chaperone;
Unfolded protein response

[†]These authors contributed equally to the work

References

[1] N.K. Karamanos, Matrix modeling and remodeling: a biological interplay regulating tissue homeostasis and diseases, Matrix Biol. (2019) 1–11 75-76.
[2] R.V. Iozzo, M.A. Gubbiotti, Extracellular matrix: the driving force of mammalian diseases, Matrix Biol. (2018) 1–9 71-72.
[3] R. Besio, Bone biology: insights from osteogenesis imperfecta and related rare fragility syndromes, FEBS J 286 (15) (2019) 3033–3056.
[4] S. Sprangers, V. Everts, Molecular pathways of cell-mediated degradation of fibrillar collagen, Matrix Biol. (2019) 190–200 75-76.
[5] M.P. Leighton, Decreased chondrocyte proliferation and dysregulated apoptosis in the cartilage growth plate are key

features of a murine model of epiphyseal dysplasia caused by a matn3 mutation, Hum. Mol. Genet. 16 (14) (2007) 1728–1741.
[6] S. Nundlall, An unfolded protein response is the initial cellular response to the expression of mutant matrilin-3 in a mouse model of multiple epiphyseal dysplasia, Cell Stress Chaperones 15 (6) (2010) 835–849.
[7] K.A. Piróg-Garcia, Reduced cell proliferation and increased apoptosis are significant pathological mechanisms in a murine model of mild pseudoachondroplasia resulting from a mutation in the C-terminal domain of COMP, Hum. Mol. Genet. 16 (17) (2007) 2072–2088.
[8] K.L. Posey, Chondrocyte-specific pathology during skeletal growth and therapeutics in a murine model of pseudoachondroplasia, J. Bone Miner Res. 29 (5) (2014) 1258–1268.
[9] J.C. Marini, Consortium for osteogenesis imperfecta mutations in the helical domain of type I collagen: regions rich in lethal mutations align with collagen binding sites for integrins and proteoglycans, Hum. Mutat. 28 (3) (2007) 209–221.
[10] K.Y. Tsang, In vivo cellular adaptation to ER stress: survival strategies with double-edged consequences, J. Cell. Sci. (123) (2010) 2145–2154 Pt 13.
[11] R.P. Boot-Handford, M.D. Briggs, The unfolded protein response and its relevance to connective tissue diseases, Cell. Tissue Res. 339 (1) (2010) 197–211.
[12] W.C.W. Chan, Activating the unfolded protein response in osteocytes causes hyperostosis consistent with craniodiaphyseal dysplasia, Hum. Mol. Genet. 26 (23) (2017) 4572–4587.
[13] T.S. Lisse, ER stress-mediated apoptosis in a new mouse model of osteogenesis imperfecta, PLoS Genet 4 (2) (2008) e7.
[14] L.S. Mirigian, Osteoblast malfunction caused by cell stress response to procollagen misfolding in α2(I)-G610C mouse model of osteogenesis imperfecta, J. Bone Miner. Res. 31 (8) (2016) 1608–1616.
[15] F. Tonelli, Crtap and p3h1 knock out zebrafish support defective collagen chaperoning as the cause of their osteogenesis imperfecta phenotype, Matrix Biol. (2020).
[16] W.A. Cabral, Substitution of murine type I collagen A1 3-hydroxylation site alters matrix structure but does not recapitulate osteogenesis imperfecta bone dysplasia, Matrix Biol. 90 (2020) 20–39.
[17] A. Forlino, New perspectives on osteogenesis imperfecta, Nat. Rev. Endocrinol. 7 (9) (2011) 540–557.
[18] F. Rauch, Osteogenesis imperfecta type V: marked phenotypic variability despite the presence of the IFITM5 c.-14C>T mutation in all patients, J. Med. Genet. 50 (1) (2013) 21–24.
[19] A. Forlino, Differential expression of both extracellular and intracellular proteins is involved in the lethal or nonlethal phenotypic variation of BrtlIV, a murine model for osteogenesis imperfecta, Proteomics 7 (11) (2007) 1877–1891.
[20] A. Gagliardi, Cytoskeleton and nuclear lamina affection in recessive osteogenesis imperfecta: A functional proteomics perspective, J. Proteomics 167 (2017) 46–59.
[21] F.S. Van Dijk, D.O. Sillence, Osteogenesis imperfecta: clinical diagnosis, nomenclature and severity assessment, Am. J. Med. Genet. A (6) (2014) 1470–1481 164A.
[22] Y. Taga, Site-specific quantitative analysis of overglycosylation of collagen in osteogenesis imperfecta using hydrazide chemistry and SILAC, J. Proteome Res. 12 (5) (2013) 2225–2232.
[23] A. Forlino, J.C. Marini, Osteogenesis imperfecta, Lancet 387 (2016) 1657–1671 (10028).
[24] N.V. Kuznetsova, Structure, stability and interactions of type I collagen with GLY349-CYS substitution in alpha 1(I) chain in a murine Osteogenesis Imperfecta model, Matrix Biol. 23 (2) (2004) 101–112.
[25] A. Forlino, Selective retention and degradation of molecules with a single mutant alpha1(I) chain in the Brtl IV mouse model of OI, Matrix Biol. 26 (8) (2007) 604–614.
[26] R. Besio, 4-PBA ameliorates cellular homeostasis in fibroblasts from osteogenesis imperfecta patients by enhancing autophagy and stimulating protein secretion, Biochim. Biophys. Acta Mol. Basis Dis. (2018) 1642–1652 1864(5 Pt A).
[27] R. Besio, Cellular stress due to impairment of collagen prolyl hydroxylation complex is rescued by the chaperone 4-phenylbutyrate, Dis. Model Mech. 12 (6) (2019).
[28] R. Gioia, Impaired osteoblastogenesis in a murine model of dominant osteogenesis imperfecta: a new target for osteogenesis imperfecta pharmacological therapy, Stem Cells 30 (7) (2012) 1465–1476.
[29] R. Morello, Osteogenesis imperfecta and therapeutics, Matrix Biol. (2018) 294–312 71-72.
[30] S.E. Papapoulos, Bisphosphonates: how do they work? Best Pract. Res. Clin. Endocrinol. Metab. 22 (5) (2008) 831–847.
[31] L.M. Ward, Alendronate for the treatment of pediatric osteogenesis imperfecta: a randomized placebo-controlled study, J. Clin. Endocrinol. Metab. 96 (2) (2011) 355–364.
[32] F. Rauch, The effects of intravenous pamidronate on the bone tissue of children and adolescents with osteogenesis imperfecta, J. Clin. Invest. 110 (9) (2002) 1293–1299.
[33] N. Bishop, Risedronate in children with osteogenesis imperfecta: a randomised, double-blind, placebo-controlled trial, Lancet 382 (9902) (2013) 1424–1432.
[34] S.E. Papapoulos, S.C. Cremers, Prolonged bisphosphonate release after treatment in children, N Eng. J. Med. 356 (10) (2007) 1075–1076.
[35] J.C. Marini, Osteogenesis imperfecta, Nat. Rev. Dis. Primers 3 (2017) 17052.
[36] G.H. Yam, Sodium 4-phenylbutyrate acts as a chemical chaperone on misfolded myocilin to rescue cells from endoplasmic reticulum stress and apoptosis, Invest. Ophthalmol. Vis Sci. 48 (4) (2007) 1683–1690.
[37] K. Ono, A chemical chaperone, sodium 4-phenylbutyric acid, attenuates the pathogenic potency in human alpha-synuclein A30P + A53T transgenic mice, Parkinsonism Relat Disord 15 (9) (2009) 649–654.
[38] L.M. van der Velden, Folding defects in P-type ATP 8B1 associated with hereditary cholestasis are ameliorated by 4-phenylbutyrate, Hepatology 51 (1) (2010) 286–296.
[39] P.V. van den Berghe, Reduced expression of ATP7B affected by Wilson disease-causing mutations is rescued by pharmacological folding chaperones 4-phenylbutyrate and curcumin, Hepatology 50 (6) (2009) 1783–1795.
[40] B. Gong, Sodium 4-phenylbutyrate ameliorates the effects of cataract-causing mutant gammaD-crystallin in cultured cells, Mol. Vis. 16 (2010) 997–1003.
[41] R.C. Rubenstein, P.L. Zeitlin, A pilot clinical trial of oral sodium 4-phenylbutyrate (Buphenyl) in deltaF508-homozygous cystic fibrosis patients: partial restoration of nasal epithelial CFTR function, Am. J. Respir. Crit. Care Med. 157 (2) (1998) 484–490.
[42] R.C. Rubenstein, M.E. Egan, P.L. Zeitlin, In vitro pharmacologic restoration of CFTR-mediated chloride transport with sodium 4-phenylbutyrate in cystic fibrosis epithelial cells containing delta F508-CFTR, J. Clin. Invest. 100 (10) (1997) 2457–2465.

[43] M.F. Gregor, G.S. Hotamisligil, Thematic review series: adipocyte biology. Adipocyte stress: the endoplasmic reticulum and metabolic disease, J. Lipid Res. 48 (9) (2007) 1905–1914.
[44] S. Granell, Obesity-linked variants of melanocortin-4 receptor are misfolded in the endoplasmic reticulum and can be rescued to the cell surface by a chemical chaperone, Mol. Endocrinol. 24 (9) (2010) 1805–1821.
[45] S. Basseri, The chemical chaperone 4-phenylbutyrate inhibits adipogenesis by modulating the unfolded protein response, J. Lipid Res. 50 (12) (2009) 2486–2501.
[46] R. Gioia, The chaperone activity of 4PBA ameliorates the skeletal phenotype of Chihuahua, a zebrafish model for dominant osteogenesis imperfecta, Hum. Mol. Genet. (2017).
[47] T.A. Enderli, Animal models of osteogenesis imperfecta: applications in clinical research, Orthop. Res. Rev. 8 (2016) 41–55.
[48] R. Brommage, C. Ohlsson, High fidelity of mouse models mimicking human genetic skeletal disorders, Front. Endocrinol. (Lausanne) 10 (2019) 934.
[49] A. Forlino, Use of the Cre/lox recombination system to develop a non-lethal knock-in murine model for osteogenesis imperfecta with an alpha1(I) G349C substitution. Variability in phenotype in BrtlIV mice, J. Biol. Chem. 274 (53) (1999) 37923–37931.
[50] E. Daley, Variable bone fragility associated with an Amish COL1A2 variant and a knock-in mouse model, J. Bone Miner. Res. 25 (2) (2010) 247–261.
[51] D.O. Sillence, D.L. Rimoin, D.M. Danks, Clinical variability in osteogenesis imperfecta-variable expressivity or genetic heterogeneity, Birth Defects Orig. Artic. Ser. 15 (5B) (1979) 113–129.
[52] K.M. Kozloff, Brittle IV mouse model for osteogenesis imperfecta IV demonstrates postpubertal adaptations to improve whole bone strength, J. Bone Miner Res. 19 (4) (2004) 614–622.
[53] J.C. Marini, Osteogenesis imperfecta: comprehensive management, Adv. Pediatr. 35 (1988) 391–426.
[54] M. Masci, Bone mineral properties in growing Col1a2 (+/G610C) mice, an animal model of osteogenesis imperfecta, Bone 87 (2016) 120–129.
[55] X. Bi, Correlations between bone mechanical properties and bone composition parameters in mouse models of dominant and recessive osteogenesis imperfecta and the response to Anti-TGF-β treatment, J. Bone Miner Res. 32 (2) (2017) 347–359.
[56] T.E. Uveges, Cellular mechanism of decreased bone in Brtl mouse model of OI: imbalance of decreased osteoblast function and increased osteoclasts and their precursors, J Bone Miner Res. 23 (12) (2008) 1983–1994.
[57] E.L. Mertz, Makings of a brittle bone: unexpected lessons from a low protein diet study of a mouse OI model, Matrix Biol. (2016) 29–42 52-54.
[58] D.J. Klionsky, Guidelines for the use and interpretation of assays for monitoring autophagy (3rd edition), Autophagy 12 (1) (2016) 1–222.
[59] L. Lei, Z. Wu, K.F. Winklhofer, Protein quality control by the proteasome and autophagy: a regulatory role of ubiquitin and liquid-liquid phase separation, Matrix Biol. (2020).
[60] S. Omari, Mechanisms of procollagen and HSP47 sorting during ER-to-Golgi trafficking, Matrix Biol (2020).
[61] D.R. Beriault, G.H. Werstuck, Detection and quantification of endoplasmic reticulum stress in living cells using the fluorescent compound, Thioflavin T, Biochim. Biophys. Acta (10) (2013) 2293–2301 1833.
[62] J.F. Bateman, Collagen defects in lethal perinatal osteogenesis imperfecta, Biochem J 240 (3) (1986) 699–708.
[63] J.F. Bateman, Substitution of arginine for glycine 664 in the collagen alpha 1(I) chain in lethal perinatal osteogenesis imperfecta. Demonstration of the peptide defect by in vitro expression of the mutant cDNA, J. Biol. Chem. 263 (24) (1988) 11627–11630.
[64] A. Stacey, Perinatal lethal osteogenesis imperfecta in transgenic mice bearing an engineered mutant pro-alpha 1(I) collagen gene, Nature 332 (6160) (1988) 131–136.
[65] A.P. Sarafova, Three novel type I collagen mutations in osteogenesis imperfecta type IV probands are associated with discrepancies between electrophoretic migration of osteoblast and fibroblast collagen, Hum. Mutat. 11 (5) (1998) 395–403.
[66] W.A. Cabral, Type I collagen triplet duplication mutation in lethal osteogenesis imperfecta shifts register of alpha chains throughout the helix and disrupts incorporation of mutant helices into fibrils and extracellular matrix, J. Biol. Chem. 278 (12) (2003) 10006–10012.
[67] C. Montessuit, J.P. Bonjour, J. Caverzasio, Expression and regulation of Na-dependent P(i) transport in matrix vesicles produced by osteoblast-like cells, J. Bone Miner Res. 10 (4) (1995) 625–631.
[68] H.C. Anderson, Matrix vesicles and calcification, Curr. Rheumatol. Rep. 5 (3) (2003) 222–226.
[69] D.R. Eyre, M.A. Weis, Bone collagen: new clues to its mineralization mechanism from recessive osteogenesis imperfecta, Calcif Tissue Int. 93 (4) (2013) 338–347.
[70] D.R. Eyre, M.A. Weis, J.J. Wu, Advances in collagen cross-link analysis, Methods 45 (1) (2008) 65–74.
[71] D.A. Hanson, D.R. Eyre, Molecular site specificity of pyridinoline and pyrrole cross-links in type I collagen of human bone, J. Biol. Chem. 271 (43) (1996) 26508–26516.
[72] K. Horiuchi, T. Tohmonda, H. Morioka, The unfolded protein response in skeletal development and homeostasis, Cell Mol Life Sci. 73 (15) (2016) 2851–2869.
[73] C.Y. Chow, The genetic architecture of the genome-wide transcriptional response to ER stress in the mouse, PLoS Genet. 11 (2) (2015) e1004924.
[74] K. Hamamura, Chondroprotective effects of Salubrinal in a mouse model of osteoarthritis, Bone Joint Res. 4 (5) (2015) 84–92.
[75] F. Coustry, Mutant cartilage oligomeric matrix protein (COMP) compromises bone integrity, joint function and the balance between adipogenesis and osteogenesis, Matrix Biol. 67 (2018) 75–89.
[76] M.H. Rajpar, Targeted induction of endoplasmic reticulum stress induces cartilage pathology, PLoS Genet. 5 (10) (2009) e1000691.
[77] L. Bianchi, Differential response to intracellular stress in the skin from osteogenesis imperfecta Brtl mice with lethal and non lethal phenotype: a proteomic approach, J. Proteomics 75 (15) (2012) 4717–4733.
[78] P.S. Kolb, The therapeutic effects of 4-phenylbutyric acid in maintaining proteostasis, Int. J. Biochem Cell. Biol. 61 (2015) 45–52.
[79] Y.H. Tang, 4-Phenylbutyric acid presents therapeutic effect on osteoarthritis via inhibiting cell apoptosis and inflammatory response induced by endoplasmic reticulum stress, Biotechnol. Appl. Biochem. 65 (4) (2018) 540–546.

[80] W. Ma, E. Goldberg, J. Goldberg, ER retention is imposed by COPII protein sorting and attenuated by 4-phenylbutyrate, Elife 6 (2017).
[81] L.A. Mullan, Increased intracellular proteolysis reduces disease severity in an ER stress-associated dwarfism, J. Clin. Invest. 127 (10) (2017) 3861–3865.
[82] F.E. Jones, 4-Sodium phenyl butyric acid has both efficacy and counter-indicative effects in the treatment of Col4a1 disease, Hum. Mol. Genet. 28 (4) (2019) 628–638.
[83] S. Takeyari, 4-phenylbutyric acid enhances the mineralization of osteogenesis imperfecta iPSC-derived osteoblasts, J. Biol. Chem. (2020).
[84] S.M. Sweeney, Candidate cell and matrix interaction domains on the collagen fibril, the predominant protein of vertebrates, J. Biol. Chem. 283 (30) (2008) 21187–21197.
[85] R. Hua, Biglycan and chondroitin sulfate play pivotal roles in bone toughness via retaining bound water in bone mineral matrix, Matrix Biol. 94 (2020) 95–109.
[86] H.W. Lee, Histone deacetylase 1-mediated histone modification regulates osteoblast differentiation, Mol. Endocrinol. 20 (10) (2006) 2432–2443.
[87] T.M. Schroeder, J.J. Westendorf, Histone deacetylase inhibitors promote osteoblast maturation, J. Bone Miner Res. 20 (12) (2005) 2254–2263.
[88] H.F. Duncan, Histone deacetylase inhibitors induced differentiation and accelerated mineralization of pulp-derived cells, J. Endod. 38 (3) (2012) 339–345.
[89] E. Hesse, Zfp521 controls bone mass by HDAC3-dependent attenuation of Runx2 activity, J. Cell Biol. 191 (7) (2010) 1271–1283.
[90] L. Bianchi, Altered cytoskeletal organization characterized lethal but not surviving Brtl+/- mice: insight on phenotypic variability in osteogenesis imperfecta, Hum. Mol. Genet. 24 (21) (2015) 6118–6133.
[91] A. Forlino, F. Tonelli, R. Besio, Steady-State and Pulse-Chase Analyses of Fibrillar Collagen, Methods Mol. Biol. (2019) 45–53 1952.
[92] J. Jeon, M.S. Lee, H.S. Yang, Differentiated osteoblasts derived decellularized extracellular matrix to promote osteogenic differentiation, Biomater Res. 22 (2018) 4.
[93] C.A. Gregory, An Alizarin red-based assay of mineralization by adherent cells in culture: comparison with cetylpyridinium chloride extraction, Anal. Biochem. 329 (1) (2004) 77–84.
[94] P.G.B. Coelho, Evaluation of dermal collagen stained with picrosirius red and examined under polarized light microscopy, An. Bras Dermatol. 93 (3) (2018) 415–418.
[95] L. Rittié, Method for picrosirius red-polarization detection of collagen fibers in tissue sections, Methods Mol Biol. 1627 (2017) 395–407.